JGR Atmospheres

RESEARCH ARTICLE
10.1029/2018JD028648

Coastal Iberia Summertime Low-Level Flow Assessed From Scatterometers

Isabel T. Monteiro[1] **and Jur Vogelzang**[2]

[1]Instituto Português do Mar e da Atmosfera (IPMA), Lisbon, Portugal, [2]Royal Netherlands Meteorological Institute (KNMI), de Bilt, The Netherlands

Key Points:
- Details of expansion fans downwind of the Iberian major capes are well visible in ASCAT-6.25 wind data
- ASCAT-6.25 and RapidSCAT wind data show that a northern and southern regime exist during intensification events over west Iberia
- ASCAT and RapidSCAT wind data show evidence of relaxation events off west Iberia

Supporting Information:
- Supporting Information S1

Correspondence to:
I. T. Monteiro,
isabel.monteiro@ipma.pt

Citation:
Monteiro, I. T., & Vogelzang, J. (2019). Coastal Iberia summertime low-level flow assessed from scatterometers. *Journal of Geophysical Research: Atmospheres*, *124*. https://doi.org/10.1029/2018JD028648

Received 12 MAR 2018
Accepted 8 FEB 2019
Accepted article online 15 FEB 2019

Abstract In summer, the prevailing northerly flow off west Iberia occasionally intensifies and weakens with significant consequences for weather conditions and marine ecology. High-resolution Advanced SCATterometer (ASCAT) wind products on a 6.25 km grid (ASCAT-6.25) were used to characterize wind maxima downwind to the major Iberian capes. Wind intensifications downwind Cape Finisterre are large and detached from the coast. They are considered as the response to a large feature in the coastal morphology. Intensifications downwind Cape Roca and Cape São Vicente are smaller and closer to the coast. These are triggered by interaction of supercritical or transcritical flow with topography. ASCAT-6.25 evening and morning passes show two distinct regimes during intensification events: a southern regime with wind maximum moving toward the coast during the day and a northern regime in which this diurnal shift is not so clear. Another aspect that distinguishes these regimes is the later occurrence of the wind maximum in the southern portion of the coast. Also, wind relaxation events can be identified in ASCAT data. These are followed by a poleward flow of warm water that interrupts the upwelling conditions over west Iberia south of 41°N. Synoptic conditions favorable for the occurrence of intensifications and relaxations were obtained from NWP models. This study was supplemented by RapidScat observations during the summers of 2015 and 2016 at different phases of the diurnal cycle. RapidScat and ASCAT wind fields in combination with NWP data confirm that wind intensifications are multiday events, clearly distinct from the sea breeze circulation.

1. Introduction

The prevailing wind regime in western Iberia during summertime is conditioned by the presence of a subtropical anticyclone over the northeast Atlantic (Azores anticyclone) and a thermal low over the Iberian Peninsula (Martins et al., 2015; Ranjha et al., 2013). Similar synoptic conditions are found along the coasts of California and Benguela (southwestern Africa). Along the Californian coast strong northerly winds are driven by the presence of the North Pacific anticyclone and a thermal low over the southwestern United States (Halliwell & Allen, 1987; Nelson, 1977). Along the Benguelan coast, the Saint Helena anticyclone in the South Atlantic and a thermal low over the Namib desert drive strong southerly winds (Nicholson, 2010). The pressure gradient established between the anticyclone in the subtropical ocean and the thermal low over the semiarid continent drives equatorward winds which induce upwelling along the coast.

Satellite observations of coastal Iberia frequently show a broad area of high wind speeds extending offshore and equatorward (Figure 1). Similar phenomena have been observed along the Californian coast (Edwards et al., 2002) and along the coast of southwestern Africa (Patricola & Chang, 2016). Near shore, the subsiding air from the subtropical anticyclone warms and dries adiabatically, forming a contrast with the cooler and moister air near the ocean surface (Burk & Thompson, 1996). The vertical air density gradient frequently induces a well-defined marine atmospheric boundary layer (MABL). This prevailing wind regime occasionally intensifies and weakens with significant consequences for marine ecology and meteorology. Wind intensifications are associated with vertical wind speed shear and convergence of the wind at low levels, causing low-level cloudiness and fog. Wind shear and low stratus have a strong impact on weather conditions and can constitute a significant hazard to aviation operations. Wind intensifications strengthen upwelling which has a positive impact on marine life due to the higher availability of nutrients in the ecosystem as well as a negative one due to the toxic characteristics of the upwelled water (Chan et al., 2008; Fewings et al., 2016). Conversely, wind relaxations weaken upwelling which affects marine ecology by a reduction of nutrients available but also by a less corrosive environment.

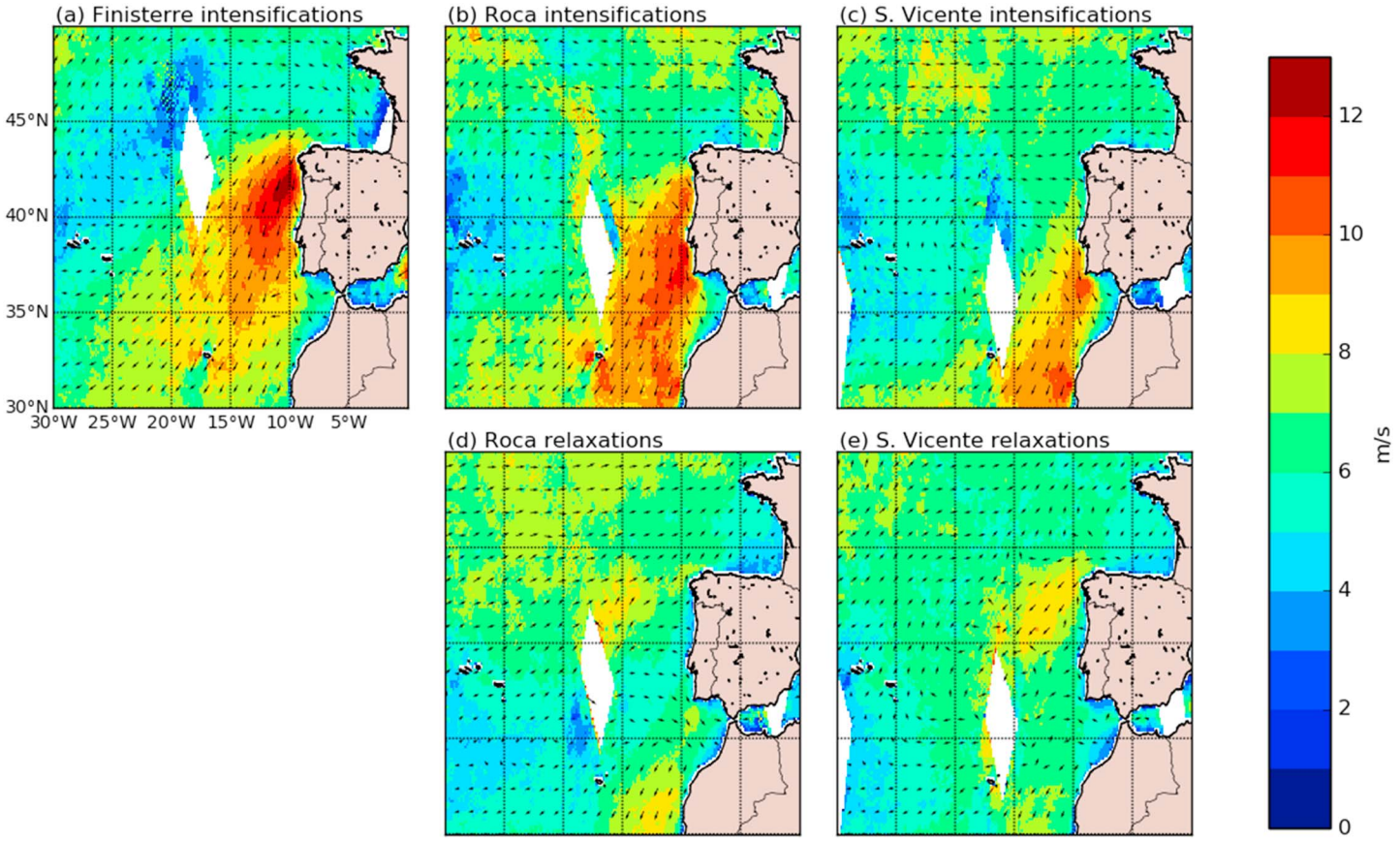

Figure 1. West Iberia 10-m mean neutral wind during Intensification events (a) Finisterre, (b) Roca, and (c) S. Vicente and relaxation events at (d) Roca and (e) S. Vicente, for June–August 2010–2014 from ASCAT-6.25. Colors indicate wind speed and arrows wind direction.

Wind intensifications produce local wind stress maxima that enhance coastal upwelling, contributing to a locally decreasing sea surface temperature (SST). The cold sea surface reinforces the air temperature inversion that caps the homogeneous cool moist MABL. If these synoptic conditions persist, a low-level coastal jet (LLCJ) is frequently produced (Burk & Thompson, 1996; Ranjha et al., 2013). In addition to this complex atmosphere-ocean coupling, the near-shore high-speed flow is further modified by its interaction with the coastal topography. For regions, as the one studied here, several authors proposed that the MABL interaction with coastal topography is explained by hydraulic theory (Monteiro, Santos, et al., 2016; Patricola & Chang, 2016; Samelson, 1992; Winant et al., 1988). Within this framework the MABL flow can be treated as the flow in a channel, the walls of which are defined by the large-scale pressure gradient offshore, the sea surface below, and the coastal mountains inland. The Froude number (Fr) for the coastal MABL is the ratio of the flow speed to the phase speed of linear gravity waves propagating on the interface between the MABL and the free atmosphere (Dorman et al., 1999):

$$Fr = \frac{V_{MABL}}{\sqrt{gH\frac{\theta_u - \theta}{\theta}}}, \tag{1}$$

where g is the gravitational acceleration, H is the average height of the MABL, θ is the air potential temperature at the MABL base, θ_u is the air potential temperature at the MABL top, and V_{MABL} is the mean speed at the MABL. When $Fr < 1$ the flow is subcritical and its mass and velocity will adjust to a perturbation both upstream and downstream. Conversely, when $Fr \geq 1$ the flow conditions are supercritical, and a perturbation in the flow, caused for example by a cape or a bend, cannot propagate upstream. Flows with both supercritical and subcritical regions are named transcritical. The hydraulic theory of Ippen (1951) explains the velocity and depth adjustment to the side walls of the channel in supercritical conditions: when the channel gets narrower because the coast line turns into the flow, the MABL thickens and its velocity decreases,

forming a compression jump or compression bulge on the upwind side. On the other hand, when approaching a "widening channel" like a coastal bend, the flow accelerates and the MABL becomes thinner, forming an expansion fan. Rogerson (1999) found a MABL behavior in transcritical coastal conditions similar to that in supercritical conditions. During wind intensifications the characteristic high-speed regions, extending for hundreds of kilometers offshore, contain smaller size intensification regions that extend tens of kilometers downwind capes and coastal bends (Chelton et al., 2004; Edwards et al., 2002; Monteiro, Santos, et al., 2016). Additionally to the interactions between the MABL and coastal topography described by the hydraulic theory, the presence of a solid channel wall inland introduces further complexity in the flow behavior. The physical consequence of this solid wall is a larger surface drag inland causing a wind drop-off toward the coast at the onshore side of the fan (Capet et al., 2004; Koračin et al., 2004). This creates a narrow band of wind speed drop-off in the vicinity of the coastline at the onshore side of fans and a much broader region of wind decrease at the other side. SST-wind coupling and several other surface processes can add to this drop-off (Renault et al., 2012). An asymmetric cross-shore wind speed profile is therefore expected, showing gradual wind weakening toward the ocean, at the western side of expansion fans, and a sharp wind drop-off toward the coast, at the eastern side. Further complexity is introduced by the fact that in real coastlines orographic features are frequently closely spaced and their effect on the flow dynamics cannot be considered separately. The distance between Cape Finisterre (Finisterre) and Cape Roca (Roca) is about 480 km, sufficient to treat the two capes independently. Conversely, the distance between Roca and Cape São Vicente (S. Vicente) is only ~200 km, and in supercritical conditions an expansion fan triggered downwind Roca can be blocked by a compression jump or bulge forming upwind S. Vicente (Monteiro, Santos, et al., 2016). Similar interaction between closely spaced capes was previously reported by Haack et al. (2001) between Cape Blanco and Cape Mendocino for the U.S. west coast. In this study, it is hypothesized that wind intensifications are mainly caused by a MABL response to hydraulic control triggered by interaction of supercritical or transcritical flow with topography. Additionally, the complexity introduced in the flow by the solid coastal wall and the interactions between capes are considered.

The prevailing summertime regime is also episodically modulated by wind weakening that causes relaxation of coastal upwelling (Oliveira et al., 2009; Washburn et al., 2011). In the Californian upwelling region these wind relaxation events can interrupt the prevailing regime within 100 km of the coast with cross-coast scales being the same as that of the wind intensifications (Fewings et al., 2016). Several authors (Garcıa-Lafuente et al., 2006; Oliveira et al., 2009; Relvas & Barton, 2002) relate warm currents along the southwestern Iberian coast to wind relaxation events. However, these studies mainly address the oceanographic consequences of wind relaxations. Our focus is on the meteorological conditions associated with these events.

As mentioned above, wind intensifications and relaxations have strong impact on the atmospheric and marine systems and consequently on weather conditions and marine ecosystems. To fully understand what triggers these modulations both synoptic and mesoscale conditions need to be assessed.

In this study synoptic information covers most of the northwest Atlantic and can be obtained with sufficient detail from NWP models like ERA-Interim from the European Centre for Medium-Range Weather Forecasts (ECMWF). For the detection of intensifications and relaxations and their detailed characterization observations are better suited because the details of such mesoscale features are rather poorly represented in NWP models as demonstrated by Monteiro, Santos, et al. (2016). As a typical example, Figure 2 shows wind fields during intensifications at Finisterre on 10 August 2015, 09:30 UTC (upper panels), Roca on 28 June 2015, 21:10 UTC (middle panels), and Vicente on 10 July 2015, 21:05 UTC (lower panels) from ASCAT-6.25 (left hand panels) and the Integrated Forecast System (IFS) of ECMWF at the smallest grid size (right hand panels). To facilitate comparison, the model data are interpolated bilinear in space and quadratic in time to the ASCAT-6.25 grid using forecast leads of 6, 9, and 12 hr.

Space-borne scatterometers are a powerful tool to study the ocean near surface wind, as they regularly provide a large number of measurements in places where conventional observations are scarce. In the inner coastal region, wind estimates from scatterometers are restrained by the distance to shore since backscatter measurements are strongly affected by the presence of land. Advances in averaging the full resolution measurements from scatterometers have improved coastal coverage, allowing one to obtain good quality winds over the sea surface as close as 15–20 km from the coast line (Verhoef et al., 2012).

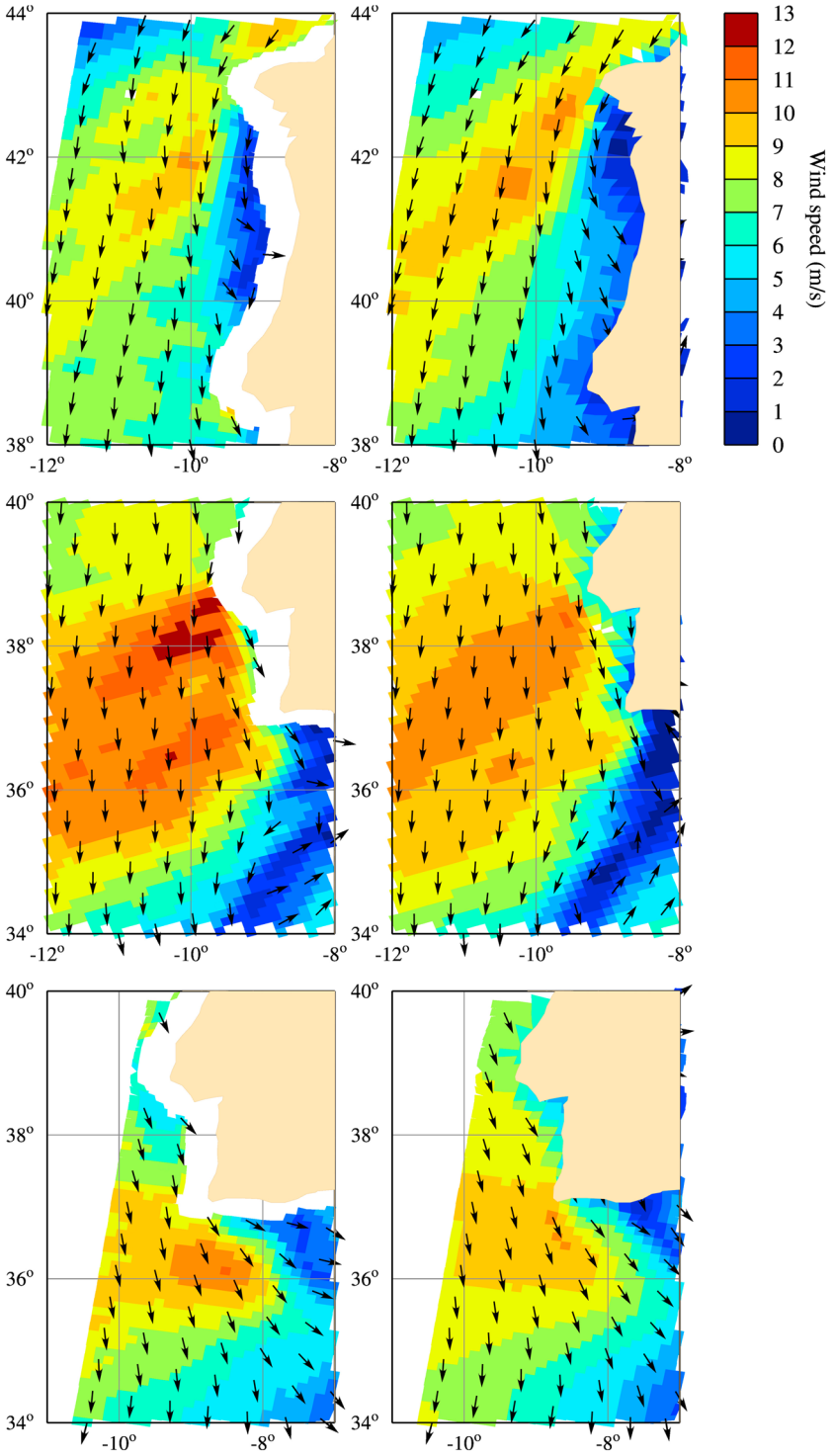

Figure 2. Ocean surface wind speed (m/s) and direction during intensification events at Finisterre on 10 August 2015, 09:30 (upper panels); Roca on 28 June 2015, 21:09 (middle panels); and S. Vicente on 10 July 2015, 09:18 (lower panels). Left hand panels show the ASCAT-6.25 wind field, right hand panels the IFS wind fields at highest resolution interpolated to the ASCAT grid. Wind direction arrows have been thinned by a factor of 4.

More recently, an ASCAT scatterometer wind product on a 6.25 km grid and with a true spatial resolution of about 17 km has become available (Vogelzang et al., 2017). In addition, scatterometer missions have long data sets. The longest continuous data records are currently available from SeaWinds onboard QuikSCAT (1999–2009; Fore et al., 2014), and the Advanced SCATterometer (ASCAT) carried by Metop-A (2007–present; Verhoef et al., 2017).

Scatterometers are usually mounted on satellites in a Sun-synchronous polar orbit, so wind observations are available only at two distinct times of the diurnal cycle for a given instrument. The RapidScat 3 years-mission (2014–2016) in a non-Sun-synchronous orbit provides different overpass times for each day over a given area.

The purpose of this study is to explore the above mentioned advances in scatterometer processing and combine them with available model data in order to improve the description of the Iberian summertime low-level coastal flow. Consistent long data sets allow a robust characterization of wind intensifications and relaxations. Model data allow characterization of the synoptic conditions favorable for the occurrence of expansion fans, while observations at high resolution give details of their surface signatures. In addition, RapidScat provides wind observations during the summers of 2015 and 2016 at times not covered by other missions, allowing one to access different phases of the diurnal cycle during wind intensifications and relaxations on an event basis.

The paper is organized as follows. The area of interest and the data used are described in section 2. In section 3 intensification and relaxation events are characterized and their frequency, temporal scales, and spatial scales are assessed. Section 4 zooms in to the spatial and diurnal variability of intensifications and relaxations. It is shown that wind speed maxima downwind Finisterre are large and detached from the coast, while downwind Roca and S. Vicente they are narrow and asymmetric. It is also shown that the diurnal variability is distinct in the northern and southern sections of the coast. The paper ends with a discussion and the conclusions in section 5.

2. Area of Interest and Data Used

2.1. Area of Interest

The Iberian west coast is located in the Northeast Atlantic and extends for about 700 km from approximately 36 to 44°N. It has several capes and coastal mountains which are generally below 1,000 m, see Figure 3. Cape Finisterre is located in the northern sector of the coast (~43°N); southward of this cape the coast bends inward up to about 41°N and then outward to Cape Roca (~38.8°N). South of Cape Roca the coastline bends 90° inland for about 25 km. Cape São Vicente is located about 200 km southward (~37°N). It is the southernmost tip of the Iberian west coast; from there the coast line is oriented west-east.

2.2. Data Used

This study covers two periods, the summers of 2010 to 2014, and the summers of 2015 and 2016. For the summers of 2010 to 2014 the following data are used:

1. ASCAT-6.25 and ASCAT-6.25 oversampled wind data to detect intensifications and relaxations;
2. ERA-Interim data to characterize the synoptic conditions under which intensifications and relaxations occur.

For the summers of 2015 and 2016 the following data are used:

1. ASCAT-coastal wind data (12.5 km grid size) to detect intensifications and relaxations;
2. RapidScat L2B Climate Ocean Wind Vectors in 12.5 km Footprints Version 2.0 to detect intensifications and relaxations at times of the day not covered by ASCAT;
3. ECMWF-IFS model forecasts at 9 and 16 km grid size to characterize the diurnal cycle along the Iberian west coast;
4. SST data to show the temperature effects of relaxations.

These data will be described in more detail in the paragraphs below.

2.2.1. Ocean Vector Winds

ASCAT has three fan-beam antennas at each side of the satellite operating at C-band (5.3 GHz). Since no moving parts are involved in the antenna design, this type of scatterometer can be operated at relatively

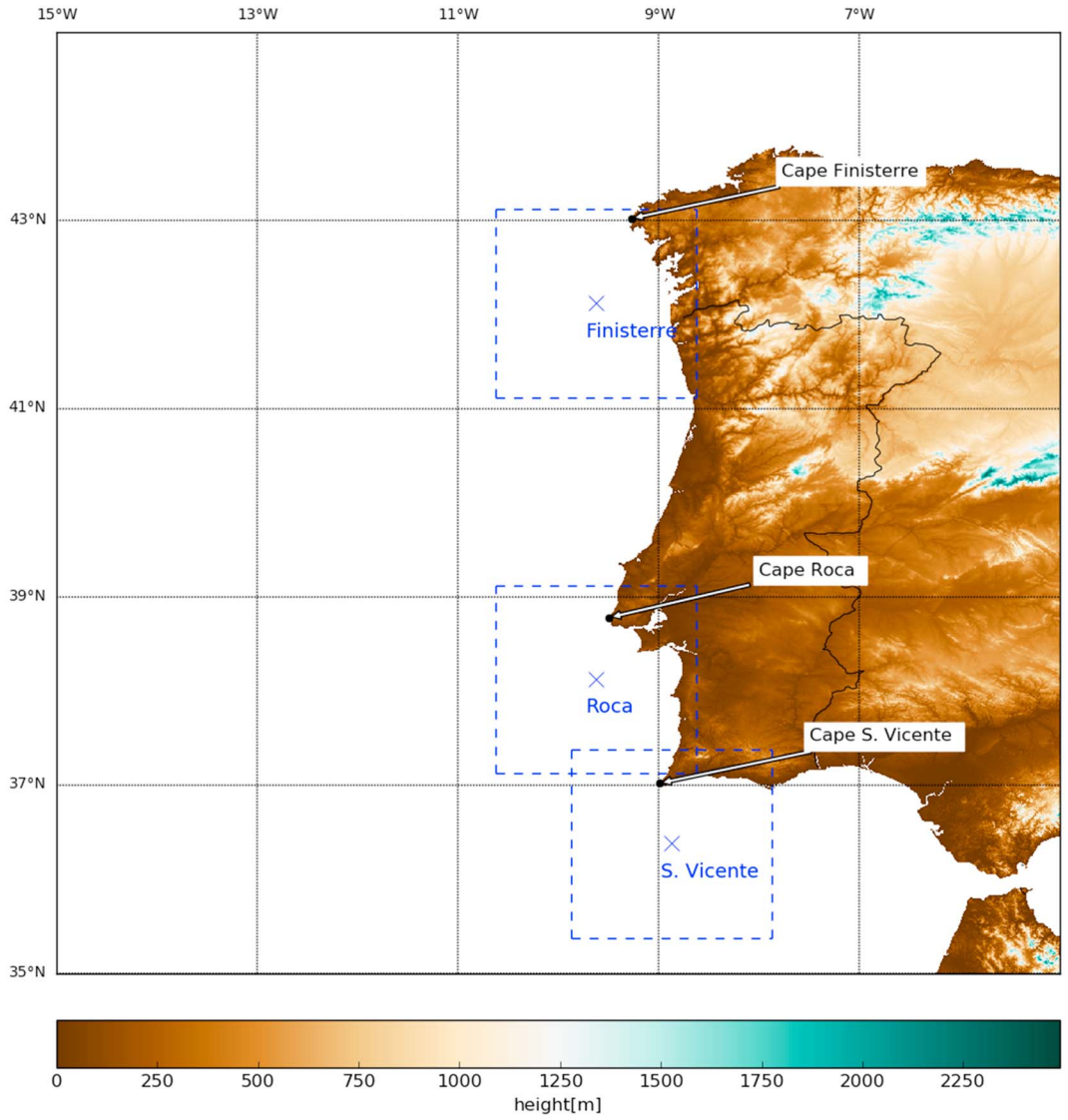

Figure 3. Map of west Iberia topography and key geographical points (Cape Finisterre, Cape Roca, and Cape S. Vicente) referred in the text. Blue crosses note locations considered to compute intensification and relaxation event statistics (Finisterre, Roca, and S. Vicente). Dashed 2° × 2° boxes note areas considered for detailed analysis.

large radar wavelengths that are almost insensitive to rain. Two swaths 550 km wide at each side of the satellite ground track are covered with a gap of about 670 km between them (Figa-Saldaña et al., 2002). ASCAT is in a sun-synchronous orbit with overpasses over the area of interest around 10:00 UTC (descending) and 22:00 UTC (ascending).

The main data set used in this study consists of ASCAT-6.25 winds for the summers of 2010 to 2014. The ASCAT-6.25 wind product was developed at the Royal Netherlands Meteorological Institute (KNMI) in the framework of the Numerical Weather Prediction Satellite Application Facility (http://www.nwpsaf.eu). This high-resolution wind product is currently not distributed operationally but has to be generated individually by users. The ASCAT wind data processor (AWDP) developed by Numerical Weather Prediction Satellite Application Facility allows presently to derive ocean vector winds on a 25, 12.5, or 6.25 km grid. ASCAT-6.25 data were obtained using the full resolution ASCAT L1B product from the European Organization for the Exploitation of Meteorological Satellites (EUMETSAT) Earth Observation portal as input. Two ASCAT-6.25 products were generated employing AWDP version 2.4 (AWDP-2.4). The first, ASCAT-6.25, was generated with an aggregation radius of 7.5 km, which offers

the best possible compromise between resolution and accuracy (Vogelzang et al., 2017). The second data set was obtained with an aggregation radius of 15 km and will hereafter be named ASCAT-6.25-oversampled. This product has the same sampling characteristics as ASCAT-coastal, but depicted on a 6.25 × 6.25 km grid. The objective of using this oversampled product was to remove collocation differences. Details on validation results of ASCAT-6.25 winds against buoys for the region and time range of the study can be found in the supporting information (more details on methodology can be found in Businger, 1973; Edson et al., 2013; Liu et al., 1979; Mears et al., 2001; Stoffelen, 1998; and Sundu et al., 2013; details on AWDP in Verhoef et al., 2018; details on validation in Monteiro, Vogelzang, & Stoffelen, 2016; and Vogelzang et al., 2017; and details on buoys data sets in http://www.puertos.es/en-us/oceanografia and http://www.hidrografico.pt/).

RapidSCAT on ISS is a Ku-band scatterometer similar to SeaWinds (Wu et al., 2003). RapidScat was operated from September 2014 until August 2016, covering the summers of 2015 and 2016. It follows a non-Sun-synchronous orbit, so its local overpass time is not constant as for ASCAT, giving wind measurements at different phases of the diurnal cycle. We used RapidScat Level 2B Climate Ocean Wind Vectors in 12.5 km Footprints Version 2.0 from the Physical Oceanography Distributed Active Archive Center (RapidScat Project, 2018).

These data were complemented with ASCAT-coastal wind products on the same grid size 12.5 km, distributed by Ocean and Sea Ice Satellite Application Facility (OSISAF) of EUMETSAT in order to characterize the diurnal cycle for selected events during the summers of 2015 and 2016.

Scatterometer winds are provided as equivalent neutral wind vectors at 10 m. Differences between neutral and actual wind depend of the presence of stable, neutral, or unstable atmospheric conditions (de Kloe et al., 2017). In summer, the prevailing regime off west Iberia correspond to stable stratified boundary layer conditions. In the particular case of 2010–2014 summers, buoy data reveal that >90% the marine boundary layer profiles corresponded to stable conditions (not shown). Nevertheless, the stability effects on wind are small, generally within the range [0, 0.3] m/s (Portabella & Stoffelen, 2009). Therefore, for the purposes of this study, scatterometer neutral winds are consider without correcting for stability effects.

2.2.2. Model Data

To document the synoptic scale conditions during summertime, ERA-Interim reanalysis data from 2010 to 2014 were employed. The advantage of ERA-Interim over the IFS is that ERA-Interim uses a fixed model version and therefore is better suited for climate applications. The grid size of the data is approximately 80 km (T255 spectral) on 60 vertical levels from the surface up to 0.1 hPa, which is sufficient for the purpose of this study. A description of the ERA-Interim reanalysis can be found in Dee et al. (2011). To characterize the synoptic conditions we calculated mean sea-level pressure (SLP) fields for all summer conditions, for wind intensifications, and for wind relaxations.

To get further insight on the MABL 3-D dynamics and diurnal cycle during wind intensifications in the summers of 2015 and 2016, model data with better resolution are needed. Therefore, the operational ECMWF IFS was used (cycles 41r1 and 41r2). These data complement the ASCAT and RapidScat observations. ECMWF/IFS (cycles 41r1 and 41r2) is a global deterministic high-resolution model of 16 and 9 km horizontal grid (T1279 spectral) on 137 vertical levels. Wind speed, potential temperature, and temperature averaged fields of 00:00 UTC forecasts, lead times 0–24 hr, were considered. Details on ECMWF/IFS global model can be found in ECMWF (2015a) and ECMWF (2015b).

2.2.3. SST Data

To document the occurrence of warm water currents associated with wind relaxations, hourly SSTs provided by OSISAF for June 2015 (http://www.osi-saf.org/) were used. OSISAF SST for this period is estimated from the Spinning Enhanced Visible and Infrared Imager onboard Meteosat-10. These data are provided at a 0.05° × 0.05° grid with 1 hr frequency. SST is estimated as a linear function of clear-sky top of the atmosphere brightness temperatures measured by Spinning Enhanced Visible and Infrared Imager split-window channels centered at 10.8 and 12.0 μm. One limitation of these SST products is that they are only retrieved under clear-sky conditions. To overcome this limitation, daily averages were computed from hourly values to reduce the number of pixels with missing values. These averages were used to identify warm water pools along the coast.

Table 1
Geographical Locations Considered to Compute Intensification and Relaxation Event Statistics and Wind speed Thresholds for Wind Intensifications and Relaxations

Location	Center latitude	Center longitude	Intensification threshold (ms^{-1})	Relaxation threshold (ms^{-1})
Finisterre	42.12	−9.625	10.5	--
Roca	38.125	−9.625	10.8	7.6
S Vicente	36.38	−8.875	10.1	7.4

3. Characterization of Wind Intensifications and Relaxations

3.1. Identification of Thresholds for Intensification and Relaxation Events

Wind speed thresholds and area boundaries for identifying Intensification events were taken from Monteiro, Santos, et al. (2016). These authors used QuikSCAT-L3 descending passes (~18:00 UTC) from the summers of 2000 to 2009 to compute intensification thresholds. For wind directions ranging from NE to NW they identified three local maxima southward of the three major Iberian capes, Finisterre, Roca, and S. Vicente. For these three locations wind intensifications events were classified as corresponding to cases with wind speeds greater than or equal to the 75th percentile. This was done separately for Finisterre, Roca, and S. Vicente. The resulting empirical thresholds are shown in Table 1 for convenience.

Wind relaxation thresholds were also found empirically using a method based on the work of Melton et al. (2009). This method considers the zero crossings of the first empirical orthogonal function of the wind velocity at coastal buoys as key value for identifying wind relaxations. Zero crossings of the empirical orthogonal function indicate that the wind velocity is below its mean value. In addition, for an event to be considered as a relaxation Melton et al. (2009) require that the wind velocity should remain below this value during 60% of the time for the next 2.5 days. In the present study the mean wind speed obtained from the QuikSCAT-L3 data set was used to define the relaxation threshold at each location. It was also required that wind speed remained below the mean during at least three out of five consecutive passes (corresponding to 2.5 days). Wind relaxations inducing warm currents along the coast do not require a specific downwelling-favorable wind direction (Fewings et al., 2016; Washburn et al., 2011), and therefore no condition was imposed on the wind direction to identify these events. The resulting thresholds are listed in the last column of Table 1.

Additionally, our study focuses on wind relaxations that occur in the central and southern portions of the coast, excluding relaxation events at Finisterre. This is justified by the lack of studies supporting the idea that warm ocean currents driven by wind relaxations reach the northern sector of the coast. Therefore, it remains an open question if these events occur in the northern sector of the Iberian coast.

3.2. Wind Intensifications

Intensification threshold values from Table 1 were used to identify wind intensification events in ASCAT-6.25 data in the summers of 2010 to 2014. We found 95 intensification events at Finisterre (15% of the overpasses), 84 at Roca (15% of the overpasses), and 155 at S. Vicente (22% of the overpasses). If we consider descending (morning) and ascending (evening) ASCAT passes separately, the number of events is greater for the evening crossings at all locations (results are summarized in Table 2). Note the higher frequency of wind intensifications at S. Vicente, particularly for evening passes (100 events, 28% of the overpasses). We will return to this in section 4.

In order to understand the large-scale atmospheric conditions during intensification events, ERA-Interim fields for all intensifications identified from the ASCAT-6.25 2010–2014 data were averaged. These averaged fields are further referred to as composites. Also, composites for average summer conditions and for wind relaxations were made.

Table 2
ASCAT-6.25 Event Intensification Statistics Downwind Each Cape

	All passes			Ascending passes			Descending passes		
Location	N	Ntot	Freq. (%)	N	Ntot	Freq (%)	N	Ntot.	Freq (%)
Finisterre	95	652	15	67	321	21	28	331	8
Roca	84	641	15	55	309	18	29	332	9
S. Vicente	155	712	22	100	354	28	55	358	15

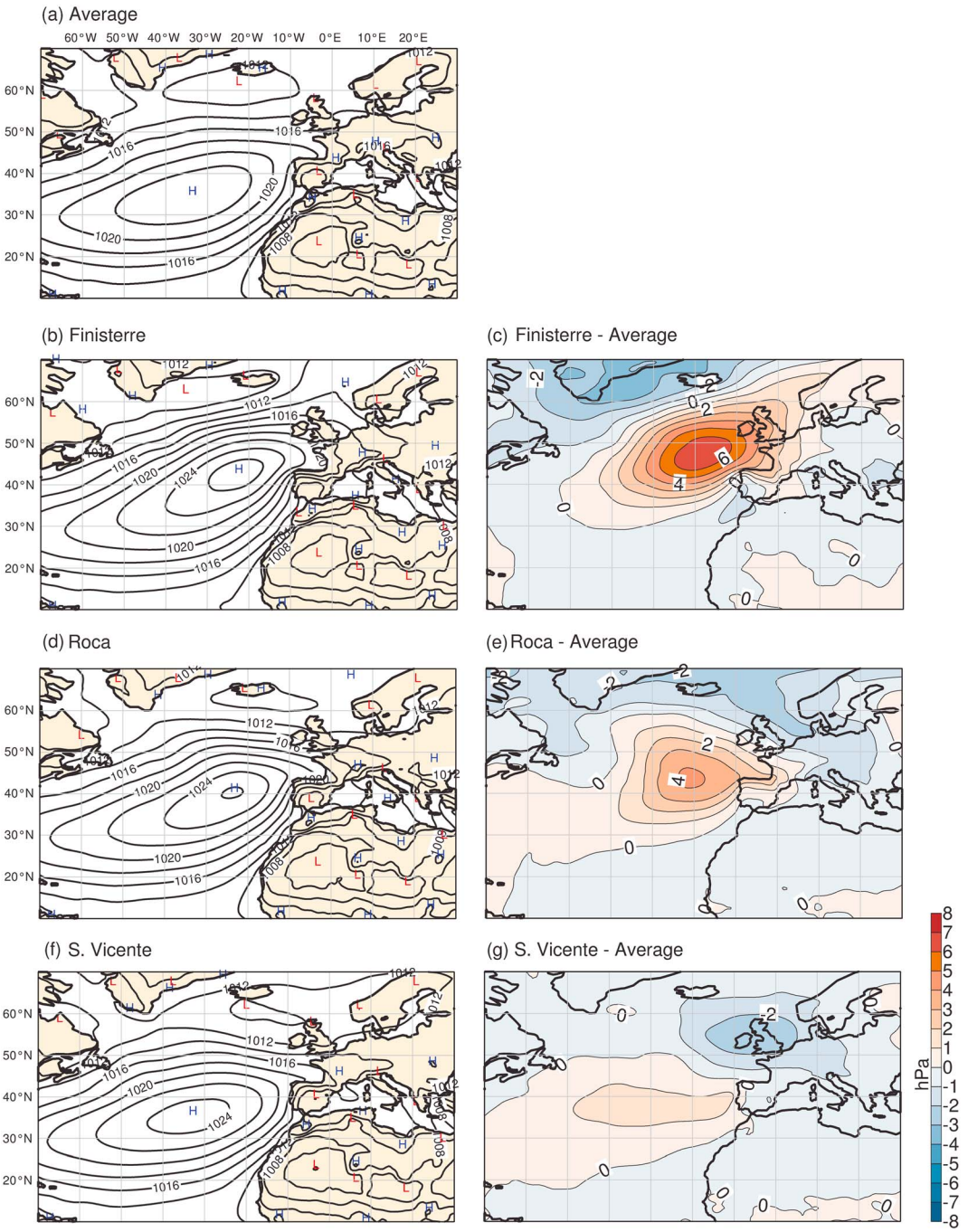

Figure 4. ERA-Interim mean SLP for (a) average summer conditions. Finisterre wind (b) intensifications and (c) anomalies. Roca wind (d) intensifications and (e) anomalies. S. Vicente wind (f) intensifications and (g) anomalies. Wind intensification events selected from ASCAT-6.25 2010 to 2014 summers. Event anomalies computed from: Event SLP minus average SLP. SLP = sea-level pressure.

Figure 4 shows ERA-Interim mean SLP and anomaly fields for average summer conditions and for wind intensifications at Finisterre, Roca, and S. Vicente, with the anomalies defined as the composite SLP field at intensification events minus the SLP field averaged over all summers of 2010 to 2014. Finisterre intensifications differ from the mean conditions by an intensification and northeastward extension of the Azores anticyclone and deepening of the thermal low over south Iberia (Figures 4b and 4c). Consequently, during Finisterre intensification events, strong pressure gradients can be found off the northwestern coast of Iberia.

Similar synoptic conditions are present for Roca intensifications (Figures 4d and 4e), but the pressure gradient maximum is located southward relative to Finisterre events. S. Vicente intensifications differ from average conditions by a deepening and southeastward movement toward the British Isles of a semipermanent low pressure system usually located over Iceland (Icelandic low). The Azores anticyclone presents a weak intensification compared to the average SLP (Figures 4f and 4g). An intensification of the pressure gradient is also present during S. Vicente events, but with the maximum located near southwest Iberia.

Influences of teleconnection patterns in the atmosphere may help to better understand the synoptic scale conditions during wind intensifications. A climate index explaining SLP patterns optimized for summer conditions along the Atlantic coast of Europe is lacking. Since the definition of such an index is out of the scope of this work we choose instead to compare ERA-Interim SLP composites from 2010 to 2014 with SLP patterns from two existing indices. The first index was proposed by Folland et al. (2009) and was developed to explain the summer conditions over the Atlantic. The second one, by Castelle et al. (2017), was optimized to winter conditions along the west coast of Europe.

Folland et al. (2009) explain Atlantic atmospheric variability in summertime circulation with a Summer North Atlantic Oscillation (SNAO). It is defined similarly to North Atlantic Oscillation as the first eigenvector of daily extratropical North Atlantic-European SLP, but in this case only during summer (July-August). Positive SNAO phases (SNAO+) are characterized by a strong extension of the Azores anticyclone over northwest Europe; negative phases (SNAO−) by a relatively southeastward displaced Iceland low.

Castelle et al. (2017), on the other hand, propose the Western Europe Pressure Anomaly (WEPA) as an optimal climate index that explains winter wave variability (related to near surface wind) along the west coast of Europe. The WEPA index is the normalized difference in SLP measured between Ireland and Canary Islands. Castelle et al. (2017) found that WEPA outscores other indices, including North Atlantic Oscillation, along the Atlantic coast of Europe from Portugal to the UK (36–52°N). Positive phases of WEPA (WEPA+) are characterized by a southern shift of the SLP anomaly between Ireland and Canary islands; negative phases (WEPA−) by a northward shift of this dipole.

SNAO explains summer conditions in the North Atlantic better than other indices, while WEPA explains the variability along the coast of Europe south of 52°N better. For the purpose of the present study it is important that both WEPA+ and SNAO− correspond to a southward shift of the North Atlantic dipole. Similarly, WEPA− and SNAO+ correspond to a northward shift of this dipole.

Comparing Figures 4c and 4e with Figure 1c in Folland et al. (2009) and with Figure 4s in Castelle et al. (2017) we conclude that Roca and Finisterre intensification events correspond to SNAO+ and to WEPA−, with the Azores anticyclone intensifying and extending over northwest Europe. S. Vicente events, on the other hand, correspond to SNAO− and WEPA+ with a relatively deep southward- and eastward-displaced Iceland low, as is clear from comparison of Figure 4g with Figure 1c in Folland et al. (2009) and Figure 4n in Castelle et al. (2017). Both the WEPA index and the SNAO index consistently show that Finisterre and Roca intensifications occur in a northern configuration of the North Atlantic dipole and that S. Vicente intensifications develop in a southern configuration of this dipole.

3.3. Wind Relaxations

The threshold values from Table 1 were used to identify wind relaxation events at Roca and S. Vicente in the ASCAT-6.25 2010-2014 summertime data set. A total number of 89 relaxation events was found during this period at Roca, and about half of this number, 43 at S. Vicente. The difference in the number of relaxation events at the two locations is mainly related to the greater persistence of weaker winds at Roca. ERA-Interim composites selected from the ASCAT-6.25 2010-2014 Roca and S. Vicente relaxation events show a large-scale attenuation of the Icelandic low and Azores anticyclone in Northeast Atlantic (Figure 5) and consequently a weaker than average SLP gradient.

To further investigate the temporal and spatial lengths involved during wind relaxations two relaxation events common at Roca and S. Vicente starting at 4 and 18 June 2015 were selected for detailed study. Time series of the wind speed were computed from the RapidScat, ASCAT-A-coastal, and ASCAT-B-coastal data for 2015 summer, for Roca and S. Vicente locations. As described in section 2.2.1, each ASCAT scatterometer has two passes over the study area whereas RapidSCAT, due to his asynchronous orbit, has a varying number of passes per day. SST time series for the same locations were derived using daily averages

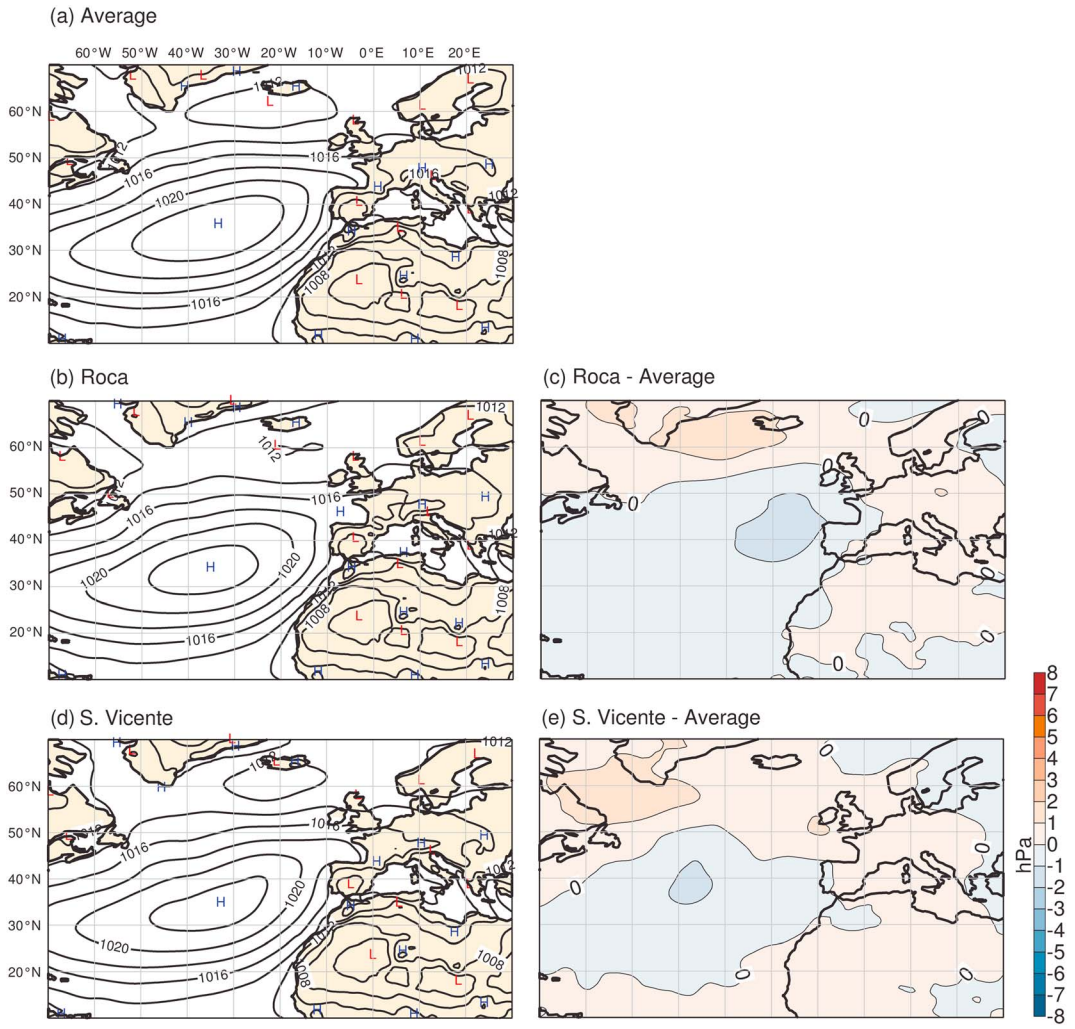

Figure 5. ERA-Interim mean SLP for (a) average summer conditions. Roca wind (b) relaxations and c anomalies. S. Vicente wind d relaxations and e anomalies. Wind relaxation events selected from ASCAT-6.25 2010 to 2014 summers. Event anomalies computed from: Event SLP minus average SLP. SLP = sea-level pressure.

computed has described in section 2.2.3. Figure 6 shows the time evolution of the two events, starting at 4 and 18 June 2015. The oceanic warm flow beginning and ending days are indicated in the upper panel; the first day of the relaxation episode is noted in the lower panel. Annotations in red refer to S. Vicente and in blue to Roca. Red and blue horizontal lines represent the S. Vicente and Roca relaxation thresholds from Table 1. At S. Vicente the first relaxation event is identifiable from 4 to 13 June 2015 (Figure 6b, red curve). It was followed by a northward flow of warm water that started on 10 June (Figure 6a, red curve). This relaxation event lasted for about 8 days and was followed by a shorter one from 18 to 23 June 2015. The first relaxation episode was observed at Roca from 7 to 15 June 2015 (Figure 6b, blue curve) and the warm poleward current was present at Roca from 15 to 19 June 2015 (Figure 6a, blue curve). The second wind relaxation was felt at Roca between 17 and 24 June 2015. The combined effect of the two events caused a warm oceanic flow along the coast that lasted until 29 June 2015 at S. Vicente (Figure 6a, red curve). The time delay between the start of the wind relaxation and the advection of warm water is about 6 to 7 days, consistent with previous studies conducted for central west Iberia using in situ and satellite data (Oliveira et al., 2009). Figure 7 shows daily averages of SST for 2 days, one during the first relaxation event and the other after the wind relaxations took place. On 15 June 2015 the propagation of the warm flow was mainly restricted to Iberian south coast while the entire west coast had SST below 20 °C (Figure 7a). Conversely, on 27 June 2015, the warm poleward flow had

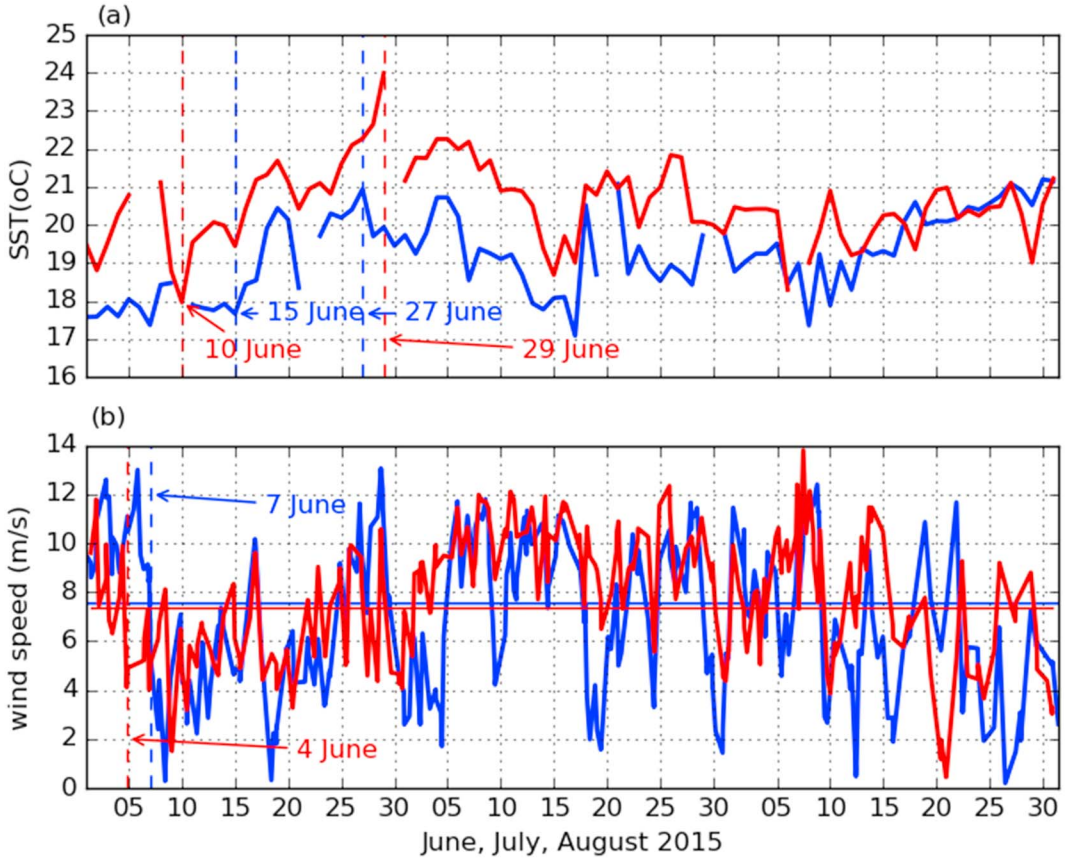

Figure 6. (a) Time series of SST and (b) wind speed at S. Vicente (red line) and Roca (blue line) for June, July, August 2015. The oceanic warm flow beginning and ending days are indicated in the upper panel; the first day of the relaxation episode is noted in the lower panel. Annotations in red refer to S. Vicente and in blue to Roca. Red and blue horizontal lines represent S. Vicente and Roca relaxation thresholds accordingly with Table 1. SST = sea surface temperature.

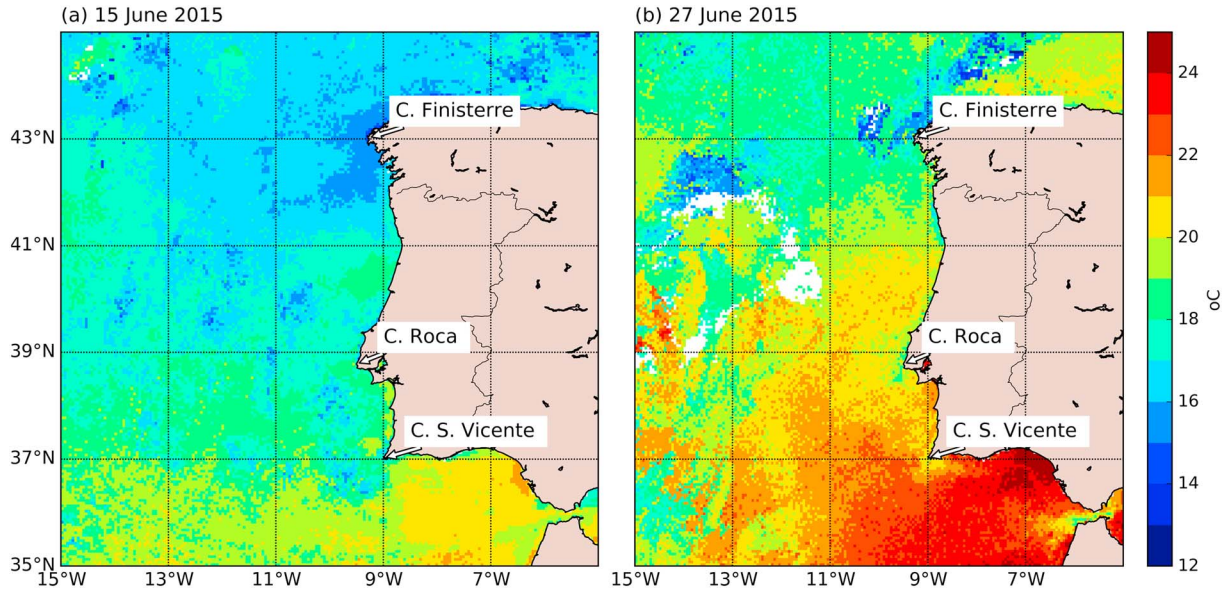

Figure 7. SEVIRI sea surface temperature for the beginning (a) and for the end (b) of the warm oceanic poleward flow, at 15 June 2015 and 27 June 2015, respectively. Copyright (2017) EUMETSAT.

already advanced up to 41°N with SST values above 20 °C over the west coast (Figure 7b). Low SST values were restricted to the northern sector of the coast showing that the relaxation event caused a disruption of the upwelling conditions over most of west Iberia.

Finally, it should be noted that ASCAT-6.25 and ASCAT-6.25 oversampled perform equally well in detecting intensifications and relaxations.

4. Spatial and Diurnal Variability of Wind Intensifications and Relaxations

4.1. Spatial Variability

As mentioned in section 1, supercritical to transcritical flow regimes are often found under high wind conditions along the entire coast of west Iberia or in portions of it. The MABL responds to the coastline topography by accelerating and thinning downwind the three major Iberian capes. Scatterometers measure the sea surface wind vector, and therefore only the surface expressions of expansion fans. These will further be referred to as fan signatures. The fan signature area is defined as a region around the location given in Table 1 where the wind speed exceeds the intensification threshold. The Finisterre fan has a typical signature area of about 16,000 km^2 and is larger than the Roca and S. Vicente fans that have a typical area of about 13,000 km^2. The signature area varies from scene to scene, and may become twice as large as the average area. The Finisterre fan signature is located more distant from shore than the Roca and S. Vicente signatures, see Figure 1a against Figures 1b and 1c. ASCAT-6.25 high-resolution wind fields show fans dimensions and spatial characteristics in great detail. It is, of course, not possible to discuss each event separately, so some averaging must be done in order to find the most characteristic features. For each fan signature, a region within a 2° by 2° box around locations given in Table 1 and depicted in Figure 3 are considered. Figure 8 shows the average horizontal cross-shore wind speed profile through the wind maximum for intensification events at Finisterre, Roca, and S. Vicente (from top to bottom) for ascending passes (left hand panels) and descending passes (right hand panels). These profiles were constructed as follows: first the wind speed maximum was found within the appropriate area of interest depicted in Figure 3. Then the average horizontal profile was updated using the row of scatterometer wind vectors containing the maximum, with the maximum at the center of the profile. The row of wind vectors is approximately perpendicular to the coast, but tilted toward the southwest for ascending passes and toward the southeast for descending passes. The direction of land and ocean is indicated at the top of Figure 8. The figure shows results for ASCAT-6.25 (solid curves) and ASCAT-6.25-oversampled (dashed curves). In all cases the ASCAT-6.25 profiles have a sharper maximum than the ASCAT-6.25-oversampled ones. This is as expected, as ASCAT-6.25 has a true spatial resolution of 17 km, while that of ASCAT-6.25-oversampled is 28 km, the same as for ASCAT-coastal (Vogelzang et al., 2017). The horizontal profiles in Figure 8 also show an asymmetric cross-shore wind speed with wind weakening toward the ocean, at the western side of an expansion fan, and a sharp wind drop-off toward the coast, at the eastern side. The wind speed decreases gradually toward the ocean, but the larger surface drag on the coastal boundary causes a sharp drop-off toward land (Capet et al., 2004; Koračin et al., 2004).

4.2. Diurnal Variability

Figure 9 shows the average position of the wind maximum during intensifications for descending (morning) and ascending (evening) passes. The maximum position was determined for each intensification event in each area taken from ASCAT-6.25, and then averaged over 1° latitude bands. Note that there is no gap between the intensification regions at Roca and S. Vicente, indicating that they sometimes merge into a single one due to the relatively small distance between them. One implication of this proximity is that the dynamical situation is more complex, because it involves the flow interaction between the two adjacent capes.

Figure 9 also shows a different behavior of ascending and descending passes in the northern and southern sectors of the coast. In the southern sector (south of 38°N) the position of the maximum moves toward the coast during the evening and away from it in the morning. This is not the case for the northern sector, north of 38°N. Such a behavior has also been identified in recent modeling studies for the Iberian west coast (Rijo et al., 2017; Soares et al., 2014), and this is confirmed here by the ASCAT-6.25 data.

ASCAT data are available only twice a day at about the same local time (around 10:00 and 22:00 UTC) and therefore these data have insufficient temporal sampling to resolve the diurnal wind variability. Due to its

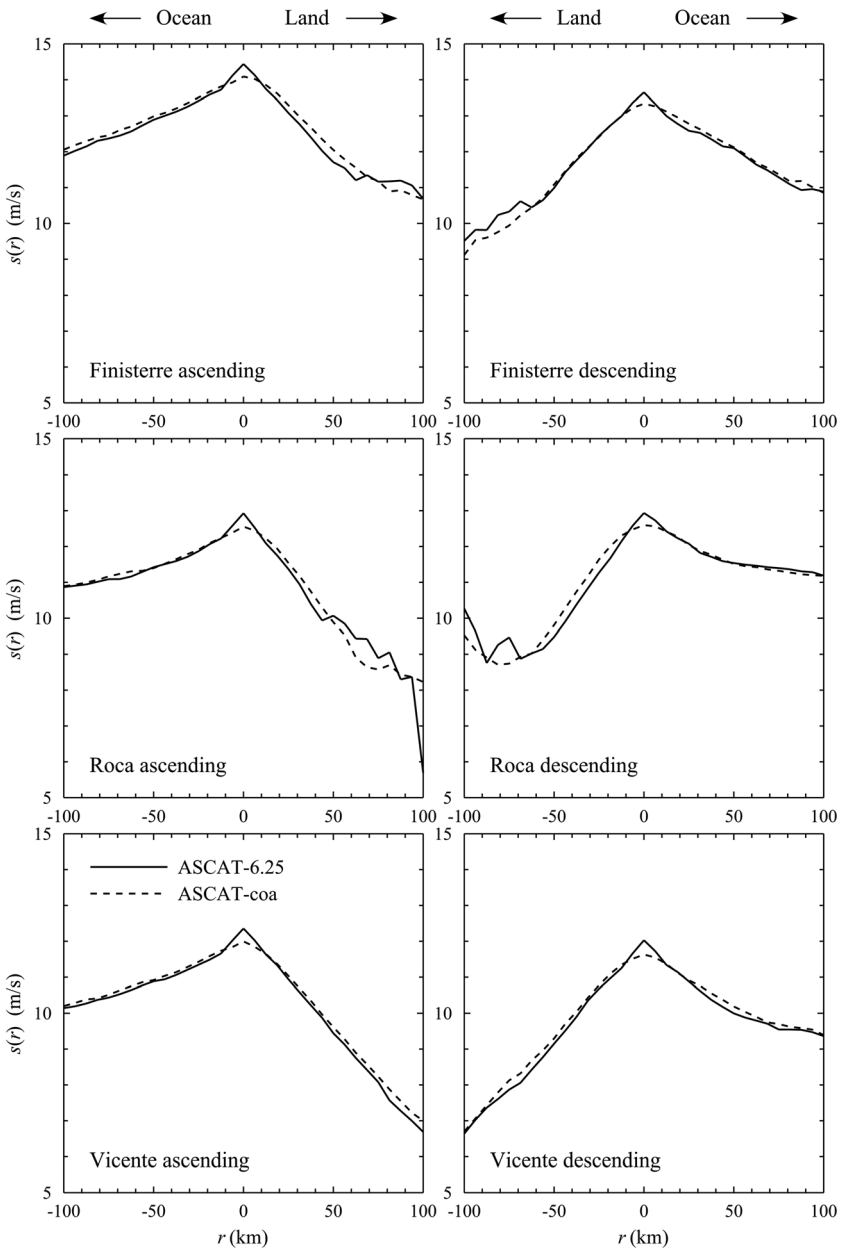

Figure 8. Average wind profiles through the wind speed maximum for Finisterre, Roca, and S. Vicente, and for ascending and descending passes.

non-Sun-synchronous orbit RapidSCAT is able to observe wind intensifications and relaxations at times of the day not accessible by ASCAT. Wind intensification and relaxation events were identified for the summers of 2015 and 2016 from RapidSCAT, ASCAT-A-coastal, and ASCAT-B-coastal, using the thresholds in Table 1. Figures 10 and 11 show the occurrence of wind intensifications and relaxations for the summers of 2015 and 2016, respectively, for Finisterre (upper), Roca (middle), and Vicente (lower). The horizontal axis gives the number of days since 1 June of the particular year, while the vertical axis gives the time of day. Each symbol represents a satellite overpass that produced valid winds in the center of each of the areas of interest, standing triangles for ASCAT-A, reversed triangles for ASCAT-B, and circles for RapidScat. The color of the symbols represents the wind conditions: red for intensifications, blue for relaxations, and gray for other conditions. The figures show that ASCAT overpasses around 10:00 and 22:00 UTC while the overpass time of RapidScat marches through the day.

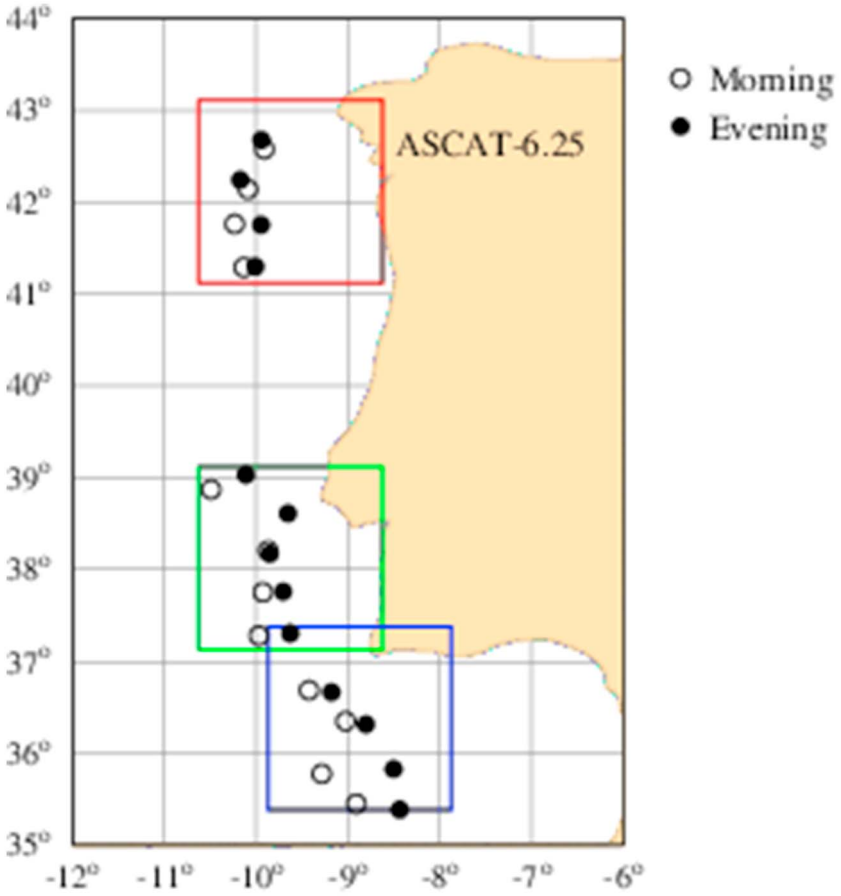

Figure 9. Mean positions of wind maxima in the morning and the evening from ASCAT-6.25 during 2010 to 2014 at Finisterre (red box), Roca (green box), and S. Vicente (blue box).

Figures 10 and 11 show that both wind intensifications and relaxations can last for entire days, as indicated by the highlighted periods (red for intensifications and blue for relaxations). Moreover, Figures 10 and 11 show for the first time for west Iberia that wind intensifications also occur at early morning and late night.

4.3. Discussion of the Diurnal Variability

Previously in this section a northern and a southern sector of the coast were identified from the distinct diurnal behavior of wind intensifications. Wind intensifications and their surface signatures are strongly linked to the boundary layer baroclinicity. Boundary layer thermodynamic conditions can vary considerably during the day. To get further insight in the structure of the MABL during these events, ECMWF/IFS event mean 3-hourly forecast fields were computed for Finisterre, Roca, and S. Vicente wind intensifications identified by ASCAT-A-coastal, ASCAT-B-coastal, and RapidSCAT using the method described in section 3.1. The results are shown in Figure 12. This figure presents the diurnal variation of the 2 years (2015 and 2016) averaged wind speed (upper panels), potential temperature (middle panels), and temperature (bottom panels). Left panels refer to Finisterre; center panels to Roca; and right panels to S. Vicente intensification events. Consistent with the findings of the previous section, wind speed maxima occur in Finisterre between 18:00 and 21:00 UTC (Figure 12a), in Roca at about 21:00 UTC (Figure 12b), and at S. Vicente between 21:00 and 03:00 UTC (Figure 12c). The MABL shows up as a region of uniform potential temperature (Figure 12 middle panels). The MABL top is recognizable as an increased gradient of potential temperature. The thermal structure above the MABL is also different from north to south. In Roca and S. Vicente the thermal inversion and a distinct MABL with a continental and warmer layer above it are present during the entire day (Figures 12h and 12i). At Finisterre (Figure 12g) these two distinct layers can only be identified in the afternoon and evening (between 12:00 and 21:00 UTC). Differences between Roca and S. Vicente are mainly related to the timing of the boundary layer diurnal cycle. At night the subsidence above the

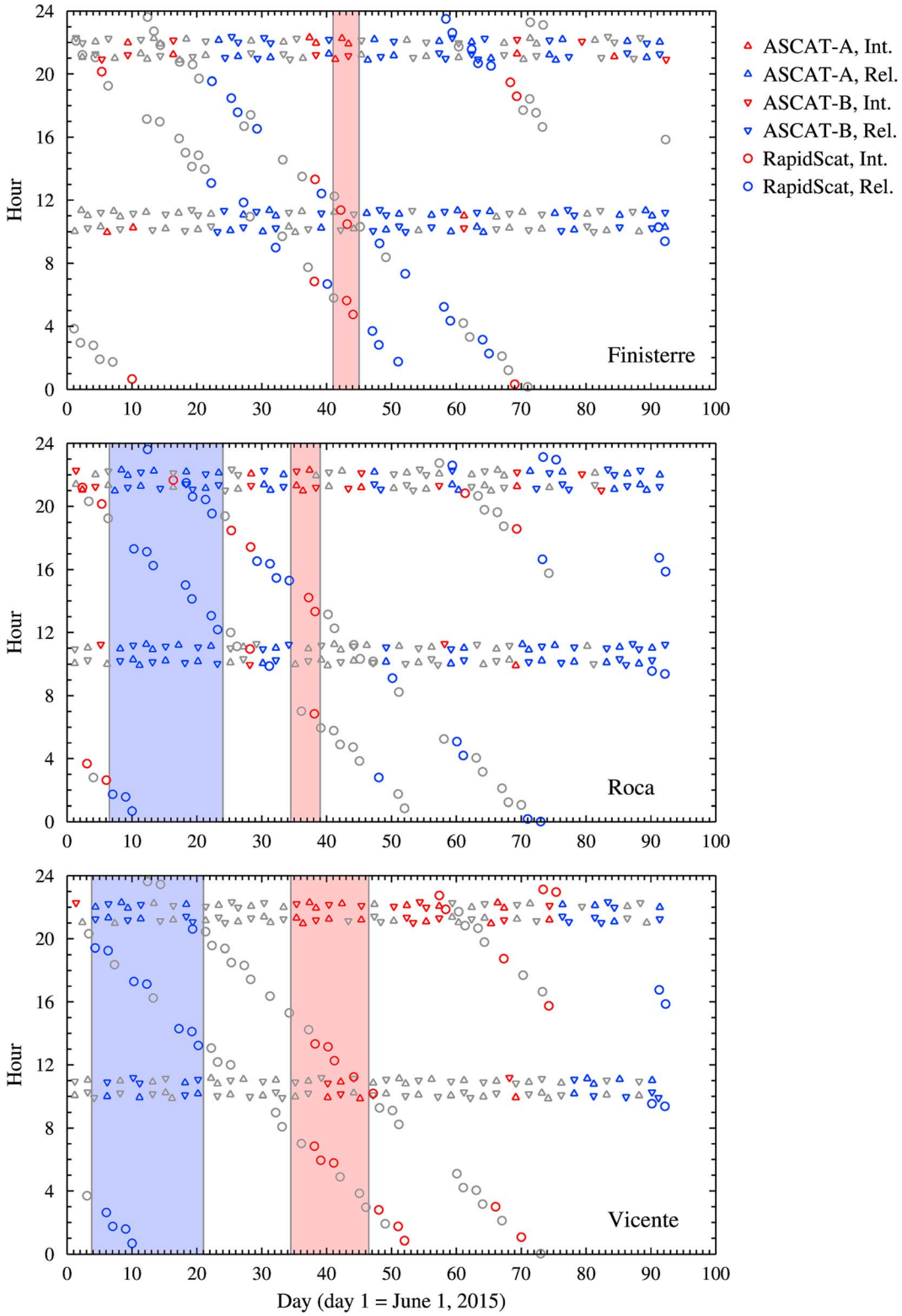

Figure 10. Event classification from ASCAT-A-coastal (standing triangles), ASCAT-B-coastal (reversed triangles), and RapidScat (circles) in summer 2015 for Finisterre (upper panel), Roca (middle panel), and S. Vicente (lower panel) as a function of day and time of day. Intensifications are in red, relaxations in blue, and other classes in gray. Highlighted in red are wind intensifications that last for entire days and in blue wind relaxations that last for more than 1 day.

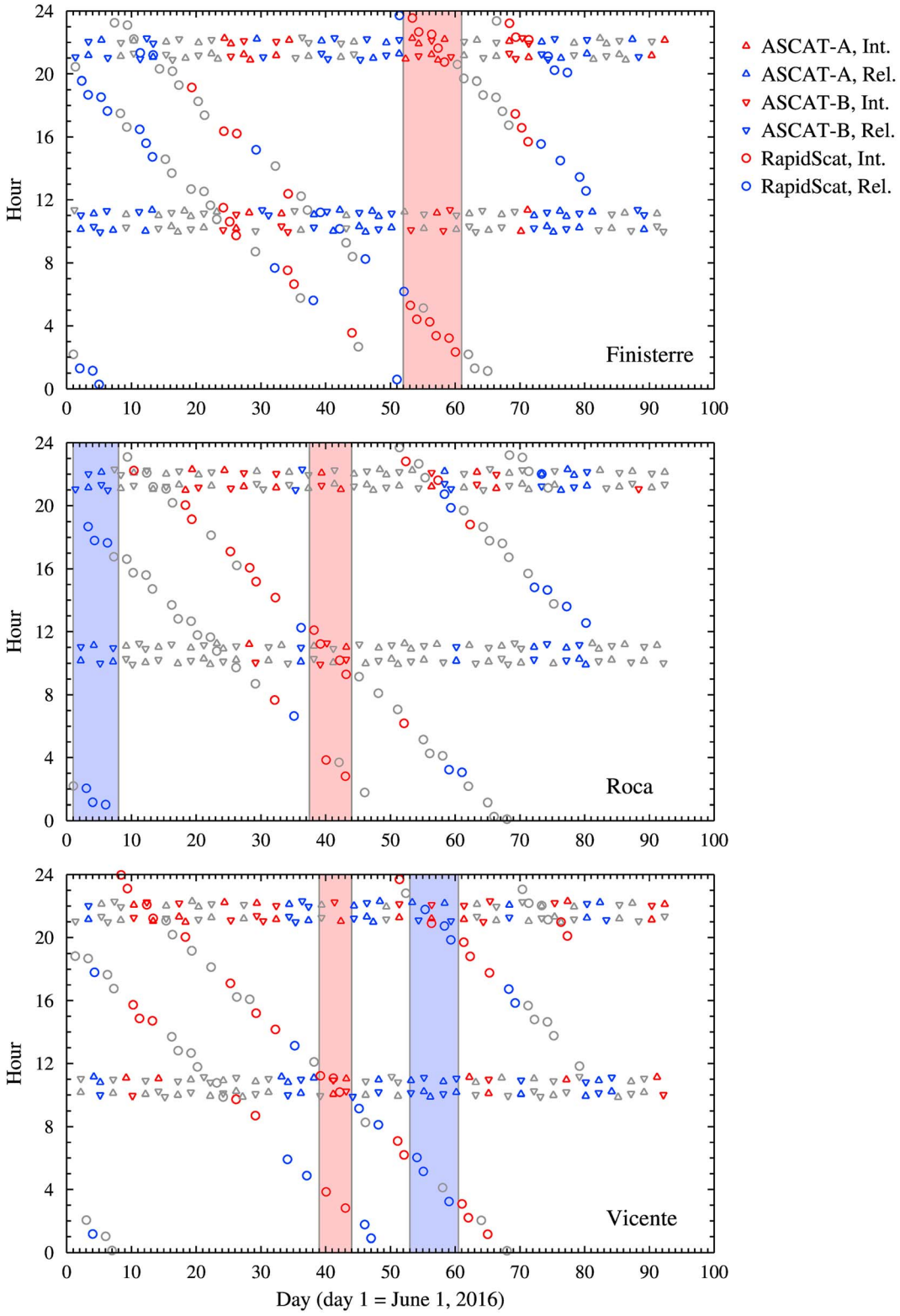

Figure 11. As Figure 10, but for summer 2016.

MABL decreases and the depth of this layer increases; during the day the opposite mechanism takes place. Compared to Roca, S. Vicente has a delayed MABL diurnal cycle. Consider a potential temperature of 290 K at Roca and of 292 K at S. Vicente as a proxy for the MABL. The maximum MABL depth at Roca occurs

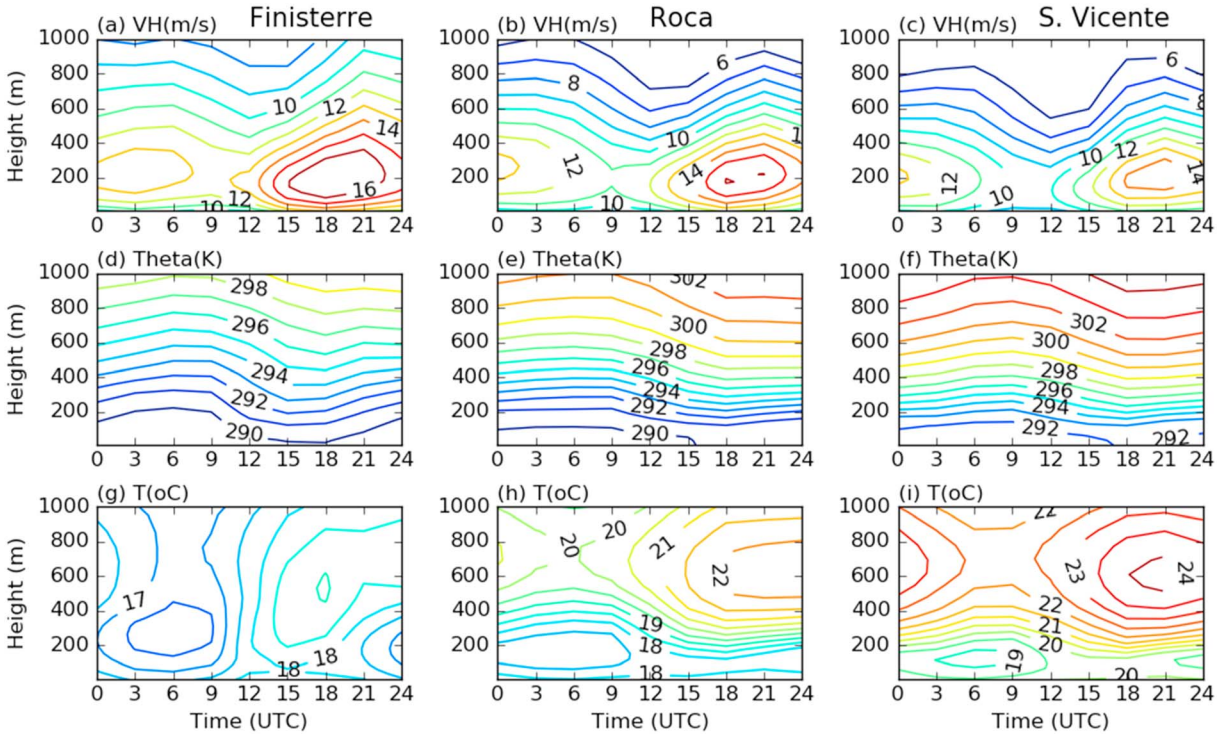

Figure 12. European Centre for Medium-Range Weather Forecasts/Integrated Forecast System averaged time series of (a–c) wind speed, (d–f) potential temperature, and (g–i) temperature. Left panels refer to Finisterre, middle panels to Roca, and right panels to S. Vicente intensification events. Averages computed for 2015 and 2016 June-July-August.

around 06:00 UTC (Figure 12e); that at S. Vicente between 09:00 and 12:00 UTC (Figure 12f). The minimum MABL depth occurs between 15:00 and 18:00 UTC at Roca and extends from 18:00 UTC up to 21:00 UTC at S. Vicente. The MABL cycle is also revealed by the diurnal cycle of temperature. At Roca, the inversion height minimum (height minimum of isotherm 18 °C) is found at about 15:00 UTC (Figures 12h). At S. Vicente the inversion height minimum (height minimum of isotherm 20 °C) is found between 18:00 and 21:00 UTC. Consistent with the greater number of the intensification events for the ascending passes for all locations (summarized in Table 2), ECMWF/IFS fields show the connection to the diurnal cycle of baroclinicity along the coast.

The fields in Figure 12 provide further insight on the distinct northern and southern regime identified in the previous section. In the southern sector (Roca and S. Vicente) the layer above the MABL top is undergoing major diurnal changes in temperature and depth, forcing the lowering and inland movement of the LLCJ (and associated surface signatures). Conversely, in the northern sector (Finisterre) the two distinct layers are not well marked and therefore the lowering and inland movement of the LLCJ does not take place. Wind intensifications as mentioned above are linked to the baroclinicity but they are not instantaneous determined by the horizontal temperature gradients (Burk & Thomson, 1996). Thus, wind intensifications are delayed relatively to the baroclinicity maximum at the jet height as well as near the surface. As the baroclinicity maximum occurs later in the southern locations the wind speed maximum also occurs later there.

This explains the observation made in section 3.2 that ASCAT-6.25 data show more frequent intensifications during the evening (ascending) passes at S. Vicente (28% of ASCAT ascending passes) than at Roca and Finisterre (about 18% and 21% of the ascending passes). Intensification frequencies have been obtained previously from QuikSCAT data by Monteiro, Santos, et al. (2016) using the same criteria as applied here. These authors find nearly the same percentage of events (about 18%) for each of the three locations. Evening passes over coastal Iberia occur at ~22:00 UTC for ASCAT and at ~18:00 UTC for QuikSCAT. Thus, although wind intensifications are in general slightly more frequent at S. Vicente, they are detected less often in QuikScat data around 18:00 UTC than in ASCAT data around 22:00 UTC because of the later wind speed maximum at S. Vicente.

5. Discussion and Conclusions

In this paper wind intensifications and relaxations of the prevailing summertime conditions along the west Iberian coast are investigated using NWP data and scatterometer winds. ASCAT-6.25 data were employed to detect intensification and relaxation events for which SLP ERA-Interim composites were constructed. Analysis of the composites shows that S. Vicente intensifications develop in a southern configuration of the North Atlantic dipole (SNAO− and WEPA+), thus in a context also favorable to the North African LLCJ. Several authors (Ranjha et al., 2013; Soares et al., 2014) reported connections between the Iberian and North African LLCJs. Our results provide further evidence of the interaction reported by those authors. Wind intensifications at Finisterre and Roca on the other hand occur on a northern configuration of this dipole (SNAO+ and WEPA−). Wind relaxations correspond simply to large-scale weakening of high and low pressure systems and consequently to weak SLP gradients over coastal Iberia. Hence, wind relaxations in western Iberia can be characterized assessing the synoptic conditions, analogously to other upwelling regions (Fewings et al., 2016).

Small differences in synoptic scale conditions during wind intensifications can trigger different mesoscale responses of the low-level flow at Finisterre, Roca, and S. Vicente (Monteiro, Santos, et al., 2016; Soares et al., 2014). For the characterization of these mesoscale responses, high-resolution scatterometer winds appear to be better suited than NWP data. From ASCAT-6.25 winds two regimes regarding intensification events were identified. The northern regime is characterized by a broad fan detached from the coast close to Finisterre. It is hypothesized that this maximum is due to the bend in Iberia coast in a similar way as reported by Edwards et al. (2002) for California and by Patricola and Chang (2016) for the Benguela region. The southern regime is characterized by the smaller Roca and/or S. Vicente expansion fans that are a hydraulic response to topography, as described for the California coast by (Dorman et al., 2013; Dorman & Koračin, 2008; Winant et al., 1988) and previously for Iberian coast by (Monteiro, Santos, et al., 2016; Rijo et al., 2017; Soares et al., 2014).

Another aspect that distinguishes these two regimes was found comparing ASCAT-6.25 morning and evening wind retrievals. In the southern region, the wind maximum approaches the coast in the evening, but this is not so clear in the northern sector. ASCAT-6.25 evening passes show wind intensification frequencies of about 21% and 18% at Finisterre and Roca, and close to 28% at S. Vicente. In a previous study using QuikSCAT during the summers of 2000 to 2009 Monteiro, Santos, et al. (2016) found that S. Vicente intensifications occur less often (18%).

The RapidScat mission yielded data at times of the day never observed before by space-borne scatterometers. During the summers of 2015 and 2016 intensification and relaxation events were identified from RapidScat and ASCAT-coastal data, both on a 12.5 km grid. In order to further investigate the different northern and southern behavior, ECMWF/IFS composites of wind speed, potential temperature, and temperature were calculated. The movement of wind intensifications toward the coast during the day has been explained by several authors as a delayed response to the daily baroclinic maximum in midafternoon (Burk & Thomson, 1996; Haack et al., 2001). During the day the boundary layer thermal structure over land varies considerably and consequently a strong diurnal variation is also present above the coastal MABL. This variation modulates the LLCJ position, intensity, and structure during the day. Consequently, wind intensifications also reflect these variations near the ocean surface. ECMWF/IFS fields show that the MABL thermal structure is not the same along the entire Iberian west coast. The northern sector has smaller thermal gradients and a distinct MABL is only clearly identifiable in the afternoon, so the diurnal modulation in the LLCJ described above does not occur. ECMWF/IFS fields also explain the higher frequency of wind intensifications at S. Vicente found from ASCAT-6.25 winds. The baroclinicity maximum at S. Vicente occurs later than in northern locations, and thus the wind maximum, which is delayed relatively to the baroclinicity maximum, occurs even later. As a consequence, QuikSCAT misses part of the more intense winds in this region. RapidSCAT data also allow us to confirm that wind intensifications (and LLCJs) are mesoscale multiday events, clearly distinct from the sea breeze circulation.

Wind relaxations are another important modulation of the prevalent wind regime favorable for upwelling. For an event that took place on June 2015 it is shown that the warm poleward flow at S. Vicente and Roca locations take place 6 to 7 days after the wind relaxation was found in ASCAT and RapidScat wind fields. For this event, the oceanic consequence was the disruption of upwelling over a large part of west

Iberia up to 41°N. These results are consistent with the ones presented previously by Oliveira et al. (2009) for the Roca region.

In general, the observations fit well into the theoretical framework outlined in the introduction. Long continuous scatterometer data records are available now and these data can be further exploited in climate studies. In addition, several scatterometer missions are planned in the coming years from EUMETSAT, Indian Research Organization, and China Meteorological Administration. These open the way to further utilize scatterometer data at different times of the diurnal cycle. Finally, advances in scatterometer data processing provide us with good quality winds closer to the coast and at finer spatial resolution, thus offering the possibility to further study mesoscale phenomena also in coastal areas.

Acknowledgments
This work has been funded by EUMETSAT in the context of the NWP SAF part of the SAF network. The contribution of I. T. Monteiro has been partly supported by EUMETSAT under the Visiting Scientist Programme. The authors wish to thank Ad Stoffelen (KNMI) for his interest in this work and stimulating discussions and Isabel F. Trigo (IPMA) for comments and suggestions regarding climate indices in section 3.2. ERA-interim data were obtained online (http://apps.ecmwf.int/datasets/data/interim-full-daily/). OSI SAF Meteosat-10 SST data were obtained online (ftp://eftp1.ifremer.fr/cersat-rt/project/osi-saf). The ASCAT L1B full resolution data were obtained from http://archive.eumetsat.int/ (products are available free of charge upon registration). AWDP software to derive ASCAT-6.25 products can be obtained free of charge upon registration at the NWP SAF website (www.nwpsaf.eu). Besides, the data used in this study can be obtained from the authors. RapidScat products were obtained from PO.DAAC (https://doi.org/10.5067/RSX12-L2C20). The buoy in situ data were obtained from Puertos Del Estado (http://www.puertos.es/en-us/oceanografia) and Instituto Hidrográfico (http://www.hidrografico.pt/) and are available under request.

References

Burk, S. D., & Thompson, W. T. (1996). The summertime low-level jet and marine boundary layer structure along the California coast. *Monthly Weather Review*, *124*, 668–686. https://doi.org/10.1175/1520-0493(1996)124<0668:TSLLJA>2.0.CO;2

Businger, J. A. (1973). Turbulent transfer in the atmospheric surface layer. In D. H. Haugen (Ed.), *Workshop on micrometeorology*, *Amer. Meteor. Soc.* (pp. 67–100).

Capet, X. J., Marchesiello, P., & McWilliams, J. C. (2004). Upwelling response to coastal wind profiles. *Geophysical Research Letters*, *31*, L13311. https://doi.org/10.1029/2004GL020123

Castelle, B., Dodet, G., Masselink, G., & Scott, T. (2017). A new climate index controlling winter wave activity along the Atlantic coast of Europe: The West Europe pressure anomaly. *Geophysical Research Letters*, *44*, 1384–1392. https://doi.org/10.1002/2016GL072379

Chan, F., Barth, J. A., Lubchenco, J., Kirincich, A., Weeks, H., Peterson, W. T., & Menge, B. A. (2008). Emergence of anoxia in the California Current large marine ecosystem. *Science*, *319*, 920. https://doi.org/10.1126/science.1149016

Chelton, D. B., Schlax, M. G., Freilich, M. H., & Milliff, R. F. (2004). Satellite measurements reveal persistent small-scale features in ocean winds. *Science*, *303*, 978–983. https://doi.org/10.1126/science.1091901

de Kloe, J., Stoffelen, A., & Verhoef, A. (2017). Improved use of scatterometer measurements by using stress-equivalent reference winds. *IEEE Journal of Selected Topics in Applied Earth Observations and Remote Sensing*, (5), 2340–2347.

Dee, D. P., Uppala, S. M., Simmons, A. J., Berrisford, P., Poli, P., Kobayashi, S., et al. (2011). The ERA-Interim reanalysis: Configuration and performance of the data assimilation system. *Quarterly Journal of the Royal Meteorological Society*, *137*(656), 553–597. https://doi.org/10.1002/qj.828

Dorman, C. E., & Koračin, D. (2008). Response of the summer marine layer flow to an extreme California coastal bend. *Monthly Weather Review*, *136*, 2894–2922. https://doi.org/10.1175/2007MWR2336.1

Dorman, C. E., Mejia, J. F., & Koračin, D. (2013). Impact of U.S. west coastline inhomogeneity and synoptic forcing on winds, wind stress, and wind stress curl during upwelling season. *Journal of Geophysical Research: Oceans*, *118*, 4036–4051. https://doi.org/10.1002/jgrc.20282

Dorman, C. E., Rogers, D. P., Nuss, W., & Thompson, W. T. (1999). Adjustment of the summer marine boundary layer around Point Sur, California. *Monthly Weather Review*, *127*, 2143–2159. https://doi.org/10.1175/1520-0493(1999)127<2143:AOTSMB>2.0.CO;2

ECMWF (2015a). Operational implementation 12 May 2015. Part III: Dynamics and numerical procedures. European Centre for Medium-Range Weather Forecasts IFS Doc. Cy41r1 (29 pp.). Retrieved from http://www.ecmwf.int/en/elibrary/9210-part-iii-dynamics-and-numerical-procedures

ECMWF (2015b). Operational implementation 12 May 2015. Part IV: Physical processes. European Centre for Medium-Range Weather Forecasts IFS Doc. Cy41r1 (213 pp.). Retrieved from http://www.ecmwf.int/sites/default/files/elibrary/2016/16648-part-iv-physical-processes.pdf

Edson, J. B., Jampana, V., Weller, R. A., Bigorre, S. P., Plueddemann, A. J., Fairall, C. W., et al. (2013). On the exchange of momentum over the open ocean. *Journal of Physical Oceanography*, *43*, 1589–1610. https://doi.org/10.1175/JPO-D-12-0173.1

Edwards, K. A., Rogers, D. P., & Dorman, C. E. (2002). Adjustment of the marine atmospheric boundary layer to the large-scale bend in the California coast. *Journal of Geophysical Research*, *107*(C12), 3213. https://doi.org/10.1029/2001JC000807

Fewings, M. R., Washburn, L., Dorman, C. E., Gotschalk, C., & Lombardo, K. (2016). Synoptic forcing of wind relaxations at Pt. Conception, California. *Journal of Geophysical Research: Oceans*, *121*, 5711–5730. https://doi.org/10.1002/2016JC011699

Figa-Saldaña, J., Wilson, J., Attema, E., Gelsthorpe, R., Drinkwater, M., & Stoffelen, A. (2002). The advanced scatterometer (ASCAT) on the meteorological operational (MetOp) platform. *Canadian Journal of Remote Sensing*, *28*(3), 404–412. https://doi.org/10.5589/m02-035./Fi

Folland, C. K., Knight, J., Linderholm, H. W., Fereday, S., Ineson, S., & Hurrell, J. W. (2009). The summer North Atlantic Oscillation: Past, present, and future. *Journal of Climate*, *22*, 1082–1103. https://doi.org/10.1175/2008JCLI2459.1

Fore, A., Stiles, B., Chau, A., Williams, B., Dunbar, R., & Rodriguez, E. (2014). Point-wise wind retrieval and ambiguity removal improvements for the QuikSCAT climatological data set. *IEEE Transactions on Geoscience and Remote Sensing*, *52*(1), 51–59. https://doi.org/10.1109/TGRS.2012.2235843

Garcıa-Lafuente, J., Delgado, J., Criado-Aldeanueva, F., Bruno, M., del Rio, J., & Vargas, J. M. (2006). Water mass circulation on the continental shelf of the Gulf of Cádiz. *Deep Sea Research, Part II*, *53*, 1182–1197. https://doi.org/10.1016/j. dsr2.2006.04.011

Haack, T., Burk, S. D., Dorman, C., & Rogers, D. (2001). Supercritical flow interaction within the Cape Blanco-Cape Mendocino orographic complex. *Monthly Weather Review*, *129*, 688–708. https://doi.org/10.1175/1520-0493(2001)129<0688:SFIWTC>2.0.CO;2

Halliwell, G. R., & Allen, J. S. (1987). The large-scale coastal wind field along the west coast of North America, 1981–1982. *Journal of Geophysical Research*, *92*(C2), 1861–1884. https://doi.org/10.1029/JC092iC02p01861

Ippen, A. T. (1951). Mechanics of supercritical flow. *Transactions of the American Society of Civil Engineers*, *116*, 268–295.

Koračin, D., Dorman, C. E., & Dever, E. P. (2004). Coastal perturbations of marine layer winds, wind stress, and wind stress curl along California and Baja California in June 1999. *Journal of Physical Oceanography*, *34*, 1152–1173. https://doi.org/10.1175/1520-0485(2004)034<1152:CPOMWW>2.0.CO;2

Liu, W. T., Katsaros, K. B., & Businger, J. A. (1979). Bulk parametrization of air-sea exchanges of heat and water vapor including the molecular constraints in the interface. *Journal of the Atmospheric Sciences*, *36*(9), 1722–1735. https://doi.org/10.1175/1520-0469(1979)036<1722:BPOASE>2.0.CO;2

Martins, J. P. A., Cardoso, R. M., Soares, P. M. M., Trigo, I., Belo-Pereira, M., Moreira, N., & Tomé, R. (2015). The summer diurnal cycle of coastal cloudiness over western Iberia using Meteosat/SEVIRI and a WRF regional climate model simulation. *International Journal of Climatology*, *36*, 1755–1772. https://doi.org/10.1002/joc.4457

Mears, C. A., Smith, D. K., & Wentz, F. J. (2001). Comparison of Special Sensor Microwave Imager and buoy-measured wind speeds from 1987 to 1997. *Journal of Geophysical Research*, *106*, 11,719–11,729.

Melton, C., Washburn, L., & Gotschalk, C. (2009). Wind relaxations and poleward flow events in a coastal upwelling system on the Central California coast. *Journal of Geophysical Research*, *114*, C11016. https://doi.org/10.1029/2009JC005397

Monteiro, I. T., Santos, A. J., Belo-Pereira, M., & Oliveira, P. B. (2016). Adjustment of the summertime marine atmospheric boundary layer to the western Iberia coastal morphology. *Journal of Geophysical Research: Atmospheres*, *121*, 3875–3893. https://doi.org/10.1002/2016JD025055

Monteiro, I. T., Vogelzang, A., & Stoffelen, A. (2016). ASCAT-6.25 validation on coastal jets-2. NWPSAF report NWPSAF-KN-VS-016. Retrieved from https://www.nwpsaf.eu/vs_reports/nwpsaf-kn-vs-016.pdf?e6316e&e6316e

Nelson, C. S. (1977). Wind stress and wind stress curl over the California current. NOAA Tech. Rep. NMFA, SSRF-714 (87pp.). [PB-273-610/6GI].

Nicholson, S. E. (2010). A low-level jet along the Benguela coast, an integral part of the Benguela current ecosystem. *Climatic Change*, *99*, 613–624. https://doi.org/10.1007/s10584-009-9678-z. 2010

Oliveira, P. B., Moita, T., Silva, A., Monteiro, I. T., & Palma, A. S. (2009). Summer diatom and dinoflagellate blooms in Lisbon Bay from 2002 to 2005: Pre-conditions inferred from wind and satellite data. *Progress in Oceanography*, *83*, 270–277. https://doi.org/10.1016/j.pocean.2009.07.030

Patricola, C. M., & Chang, P. (2016). Structure and dynamics of the Benguela low-level coastal jet. *Climate Dynamics*. https://doi.org/10.1007/s00382-016-3479

Portabella, M., & Stoffelen, A. C. M. (2009). On scatterometer ocean stress. *Journal of Atmospheric and Oceanic Technology*, *26*(2), 368–382. https://doi.org/10.1175/2008JTECHO578.1

Ranjha, R., Svensson, G., Tjernstrom, M., & Semedo, A. (2013). Global distribution of coastal low-level jets derived from ERA-Interim reanalysis. *Tellus*, *65*, 20412. https://doi.org/10.3402/tellusa.v65i0.20412

RapidScat Project. (2018). RapidScat Level 2B Climate Ocean Wind Vectors in 12.5km Footprints Version 2.0. PO.DAAC, CA, USA. Dataset accessed Nov 2018 at https://doi.org/10.5067/RSX12-L2C20

Relvas, P., & Barton, E. D. (2002). Mesoscale patterns in the Cape S~ao Vicente (Iberian Peninsula) upwelling region. *Journal of Geophysical Research*, *107*(C10), 3164. https://doi.org/10.1029/2000JC000456

Renault, L., Dewitte, B., Marchesiello, P., Illig, S., Echevin, V., Cambon, G., et al. (2012). Upwelling response to atmospheric coastal jets off central Chile: A modeling study of the October 2000 event. *Journal of Geophysical Research*, *117*, C02030. https://doi.org/10.1029/2011JC007446

Rijo, N., Semedo, A., Miranda, P. M. A., Lima, D. C. A., Soares, P. M. M., & Cardoso, R. M. (2017). Spatial variability of the Iberian Peninsula coastal low-level jet. *International Journal of Climatology*, *38*, 1605–1622. https://doi.org/10.1002/joc.5303

Rogerson, A. M. (1999). Transcritical flows in the coastal marine atmospheric boundary layer. *Journal of the Atmospheric Sciences*, *56*, 2761–2779. https://doi.org/10.1175/1520-0469(1999)056<2761:TFITCM>2.0.CO;2

Samelson, R. M. (1992). Supercritical marine-layer flow along smoothly varying coastline. *Journal of the Atmospheric Sciences*, *49*(17), 1571–1584. https://doi.org/10.1175/1520-0469(1992)049<1571:SMLFAA>2.0.CO;2

Soares, P. M. M., Cardoso, R. M., Semedo, A., Chinita, M. J., & Ranjha, R. (2014). Climatology of the Iberia coastal low-level wind jet: Weather research forecasting model high-resolution results. *Tellus*, *66*, 22377. https://doi.org/10.3402/tellusa.v66.22377

Stoffelen, A. (1998). Toward the true near-surface wind speed: Error modeling and calibration using triple collocation. *Journal of Geophysical Research*, *103*(C4), 7755–7766. https://doi.org/10.1029/97JC03180

Sundu, I., Beljaars, A., Bechtold, P., Mauritsen, T., & Balsamo, G. (2013). Why is it so difficult to represent stably stratified conditions in numerical weather prediction (NWP) models? *Journal of Advances in Modeling Earth Systems*, *5*, 117–133. https://doi.org/10.1002/jame.20013

Verhoef, A., Portabella, M., & Stoffelen, A. (2012). High-resolution ASCAT scatterometer winds near the coast. *IEEE Transactions on Geoscience and Remote Sensing*, *50*(7), 2481–2487. https://doi.org/10.1109/TGRS.2011.2175001

Verhoef, A., Vogelzang, J., Verspeek, J., & Stoffelen, A. (2017). Long-term scatterometer wind climate data records. *IEEE Journal of Selected Topics in Applied Earth Observations and Remote Sensing*, *10*(5), 2186–2194. https://doi.org/10.1109/JSTARS.2016.2615873

Verhoef, A., Vogelzang, J., Verspeek, J., & Stoffelen, A. (2018). AWDP user manual and reference guide gersion 3.2. Document NWPSAF-KN-UD-005, EUMETSAT, Darmstadt, Germany. Retrieved from https://www.nwpsaf.eu/site/download/documentation/scatterometer/AWDP/NWPSAF-KN-UD-005_AWDP_User_Guide_v3.2.pdf?e6316e&e6316e

Vogelzang, J., Stoffelen, A., Lindsley, R. D., Verhoef, A., & Verspeek, J. (2017). The ASCAT-6.25-km wind product. *IEEE Journal of Selected Topics in Applied Earth Observations and Remote Sensing*, *10*(5), 2321–2331. https://doi.org/10.1109/JSTARS.2016.2623861

Washburn, L., Fewings, M. R., Melton, C., & Gotschalk, C. (2011). The propagating response of coastal circulation due to wind relaxations along the central California coast. *Journal of Geophysical Research*, *116*, C12028. https://doi.org/10.1029/2011JC007502

Winant, C. D., Dorman, C. E., Friehe, C. A., & Beardsley, R. C. (1988). The marine layer off northern California: An example of supercritical channel flow. *Journal of the Atmospheric Sciences*, *45*, 3588–3605. https://doi.org/10.1175/1520-0469(1988)045<3588:TMLONC>2.0.CO;2

Wu, C. L., Liu, Y., Kellogg, K. H., Pak, K. S., & Glenister, R. L. (2003). Design and calibration of the SeaWinds scatterometer. *IEEE Transactions on Aerospace and Electronic Systems*, *39*, 94–109.